ACS Macro Letters

pubs.acs.org/macroletters Letter

Biomimetic Hydrogels from Mixed Gellan Gum and Tryptophan Zipper Self-Assembling Peptides

Riddhesh Doshi, Dhushanthan Mohanathas, Md. Shariful Islam, Juanfang Ruan, Richard D. Tilley, and Kristopher A. Kilian*

Cite This: ACS Macro Lett. 2025, 14, 679−686 Read Online

ACCESS | Metrics & More | Article Recommendations | Supporting Information

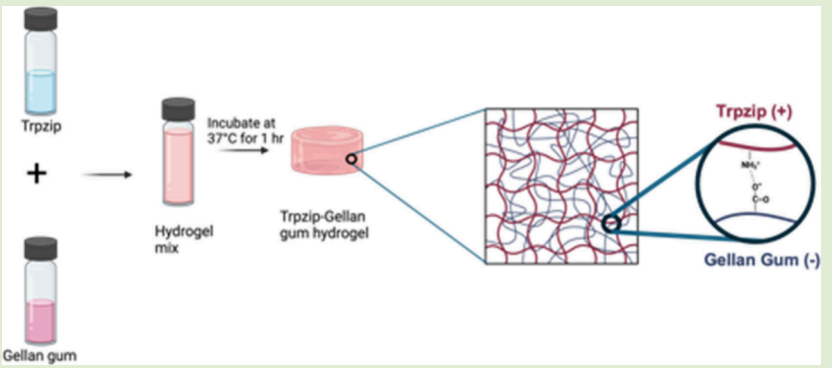

ABSTRACT: Peptide self-assembly has been used to fabricate synthetic hydrogels that emulate many of the chemical and physical properties of natural hydrogels. However, these materials often lack stability for many applications and do not display the native bioactivity found in tissue. Here we demonstrate a hybrid hydrogel system in which self-assembling peptides are integrated with polysaccharides to enhance gelation and provide improved mechanics and bioactivity. A peptide based on the tryptophan zipper (trpzip) motif was mixed with the anionic polysaccharide gellan gum, demonstrating gelation within minutes with increased stiffness compared to that of trpzip alone. The hybrid material maintained viscoelastic character with shear-thinning, self-healing, and stress−relaxation on the order of natural materials like collagen. All hydrogels supported cell adhesion and viability with increased gellan gum content, promoting cell assembly into aggregates. The enhanced gelation kinetics, stability, self-healing, and bioactivity of these materials make them promising candidates as matrices for cell culture and reagents for biofabrication and syringe extrusion for biological delivery.

Hydrogels can be split into classes of natural and synthetic origin, each with their own unique properties. The benefit of synthetic hydrogels is that their chemical and physical properties are well defined and controllable, without the need for isolation from animal sources or from patient tissue.[1] On the other hand, natural hydrogels often display a more successful outcome for integrated cells and tissues due to their inherent bioactivity.[2−4] However, the issue with natural hydrogels is that it is challenging to link biochemical and biophysical properties to the behaviors of the cells. The use of hybrid hydrogels which are composed from both natural and synthetic components has been shown to be a promising approach as it includes the desirable features of both classes.[5−8]

Designing hybrid hydrogels is often as simple as physically mixing natural and synthetic components, such as the pores of PLGA being filled by collagen.[9] There have been many examples of mixing proteinaceous materials with synthetic mesh works, where the structural stability afforded by the covalent network enhances the architecture and bioactivity of the integrated natural network.[10−13] However, they can also occur through more complex approaches which involve the orthogonal crosslinking of natural and synthetic components, such as forming double network hydrogels using covalently linked synthetic polymers and ionically crosslinked polysaccharides.[14,15,18] While these approaches are promising, there are limitations to the use of covalent networks that fail to mimic the viscoelasticity of natural materials.

A promising class of hydrogel forming materials are supramolecular networks of self-assembling peptides[16−18] because relatively simple peptide reagents can be designed to provide complex architectures with mechanical properties akin

Received: February 3, 2025
Revised: April 28, 2025
Accepted: April 29, 2025
Published: May 9, 2025

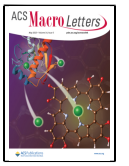

https://doi.org/10.1021/acsmacrolett.5c00076
ACS Macro Lett. 2025, 14, 679−686

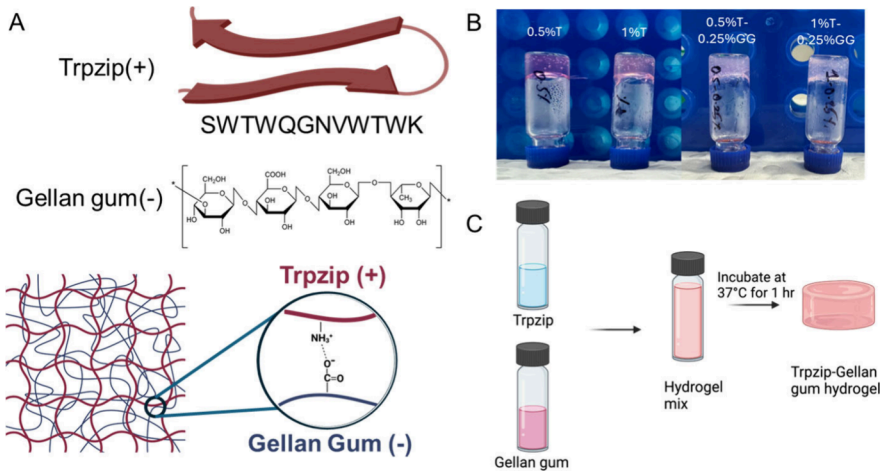

Figure 1. Forming hybrid trpzip−gellan gum (GG) hydrogels. A. Schematic representations of trpzip and gellan gum. B. Photographs of inversion test demonstrating hydrogel formation. C. Scheme for forming hybrid hydrogels.

to native tissues. These approaches invariably lead to peptide nanofibers that provide porosity for cell infiltration and can be decorated with cell adhesion motifs. Some examples of peptide-based hydrogel forming materials are short hydrogelators facilitated by hydrophobic capping groups,[19] peptide amphiphiles,[20] ionic gelators,[21] beta-hairpin forming sequences,[22,23] and sequences that mimic protein secondary structures.[24,25] While versatile reagents, peptide-based self-assembling hydrogels often lack the mechanical integrity required for many applications.

Recently, hybrid networks have been demonstrated, where the self-assembling peptide is supported by a secondary network. For instance, incorporation of FMOC peptide nanofibers into alginate networks improved mechanical properties and controlled release of small molecules.[26,27] Other examples include double network hydrogels of RADA16 and PEG, which promote improved toughness and cell adhesion, and I_3K peptide mixed with PNIPAM-based thermo-responsive hydrogels to mimic native ECM.[28] Recently, we showed how a self-assembling peptide based on the tryptophan zipper (trpzip) could be added to PEG-based hydrogels, thereby providing expanded mechanical attributes and some bioactivity to resident cells. In these hybrid networks, the bulk mechanical properties were dictated by the covalent PEG skeleton, which poses some limitations with respect to viscous traits and self-healing potential.[5]

In this communication, we report a new class of hybrid hydrogel, where a cationic beta-hairpin forming trpzip peptide is formed in the presence of the anionic polysaccharide gellan gum (Figure 1), thereby providing a viscoelastic hydrogel with unique mechanical attributes and cytocompatibility. The gellan gum serves as an ionic trigger, leading to rapid gelation and formation of a hybrid network with increased modulus and yield point, while maintaining self-healing, shear thinning, and stress−relaxation behavior. While trpzip gels alone provide a matrix for single cell spreading, integrating gellan gum was found to promote cell assembly into aggregates while maintaining high viability. Together, this new class of hybrid polysaccharide/self-assembling peptide network shows promise as a viscoelastic matrix for 3D cell culture and biomedical applications.

Trpzip will form nanofibers when dissolved in water; however, an ionic trigger is required for a higher order assembly into a hydrogel structure. Considering trpzip gelation takes 12−24 h depending on temperature, we reasoned that addition of an anionic polysaccharide could enhance the kinetics of gel formation. To explore this approach, we dissolved trpzip in water, 1−2% (w/v), and gellan gum in cell culture media, 0.5% (w/v) followed by mixing. Higher concentrations of gellan gum discouraged mixing and led to instability and phase separation. After testing these concentrations of the composite hydrogels, it was found that 0.5% trpzip−0.25% gellan gum (w/v) and 1% trpzip−0.25% gellan gum (w/v) were the two blends which formed the most stable gels per visual inspection (Figure 1B).

To evaluate the mechanical properties and viscous nature of the hydrogels, *in situ* shear rheology was performed at 0.5% T, 1% T, 0.5% T−0.25% GG, and 1% T−0.25% GG (trpzip = T; gellan gum = GG). Time sweep analysis shows that gelation of trpzip alone (0.5% T, G'= 0.886 kPa and 1% T = 2.296 kPa) takes up to 12 h to stabilize at 37 °C (Figure 2A). Addition of GG to trpzip led to gelation within 2 h for both formulations and a 1.46-fold (0.5% T−0.25%GG, G'= 1.298 kPa) and 6.41-fold (1% T−0.25% GG, G' = 12.60 kPa) increase in storage modulus. To further confirm whether gellan gum acts as an ionic trigger, trpzip-GG hydrogels were formed with and without ions (Figure S7) where trpzip and GG dissolved on mixing form stable hydrogels after 2 h. Time sweep analysis of trpzip-GG hydrogels in water and cell culture media also demonstrates that addition of gellan gum to trpzip causes rapid gelation (Figure S3). Zeta potential measurements display that the addition of gellan gum to an increasing concentration of trpzip hydrogels causes a decrease in the zeta potential of trpzip-GG hydrogels regardless of ionic buffers (Figure 2B). These results clearly indicate that gellan gum enhanced trpzip's gelation, with evidence for stabilization through electrostatic interactions between the negatively charged gellan gum polysaccharide and the positively charged trpzip peptide.

Strain sweeps revealed information about the hydrogels' yield point and crossover point, which is necessary in identifying the force required to break the hydrogels apart (i.e., demonstrates the linear viscoelastic region (LVE)). By performing strain sweeps, the gels' behavior of rapidly fluidizing after exposure to an external force was able to be quantitatively assessed. The yield point, also termed yield stress, is a shear stress limit at the linear viscoelastic region.

https://doi.org/10.1021/acsmacrolett.5c00076
ACS Macro Lett. 2025, 14, 679−686

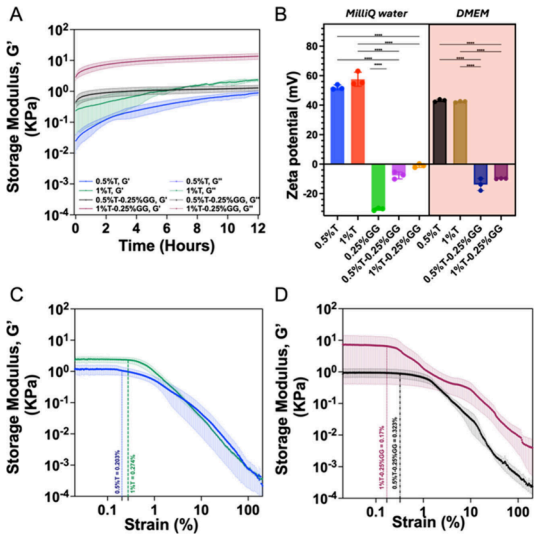

Figure 2. Shear rheological assessment of hydrogel formation. A. Time sweep demonstrating faster gelation kinetics with gellan gum (GG) addition, $n = 3$. B. Change in zeta potential on addition of gellan gum to trpzip hydrogels with and without cell culture media. *P*-values calculated using one-way ANOVA, $*P < 0.05$, $**P < 0.01$, $***P < 0.001$, $****P < 0.0001$, $n = 3$. C. Strain sweep showing increase in modulus with increased trpzip concentration, $n = 3$. D. Strain sweep showing increase in modulus and yield point for hybrid trpzip-GG hydrogels, $n = 3$. Dotted lines indicate yield-points. Shaded regions on curves indicate standard deviations between triplicate measurements.

The yield point of trpzip hydrogels is seen at a shear strain of 0.2% (equivalent to a shear stress of approximately 70 Pa). However, for the trpzip composite hydrogels, the yield points increased to 0.323% for the 0.5% T − 0.25% GG hydrogel (equivalent to a shear stress of approximately 90 Pa) (Figure 2C). This result shows how the addition of GG can stabilize the architecture, leading to an increase in the yield point. However, adding more trpzip was shown to destabilize the network and cause a decrease in the yield point (Figure 2D).

Understanding the viscous nature of hydrogels is important for applications like bioprinting and delivery via syringe. We measured the complex viscosity as a function of shear rate, observing similar shear-thinning behavior for all materials, with an increase in viscosity corresponding to an increase in material content (Figure 3A). We also measured the stress−relaxation time of the hydrogels, an important attribute of natural matrices that can guide complex biological properties.[29,30] Covalently cross-linked polymer networks which are commonly used as mimics of the ECM like poly(ethylene glycol) (PEG) do not display this behavior; however, trpzip hydrogels have been shown to exhibit stress−relaxation comparable to natural gels like collagen and Matrigel. To determine whether the addition of a polysaccharide would affect the stress relaxing behavior, constant shear deformation measurements were performed and then compared to the stress−relaxation half-time of the standalone trpzip hydrogels (Figure 3B). The stress−relaxation half times of the trpzip hydrogels were found to be approximately 33 s, while the hybrid gels showed stress−relaxation half times of approximately 40 s. This is comparable to time scales observed in collagen at ∼40 s[31] and matrigel at 87.1 s.[22] Thixotropic analyses were also performed to determine how the polysaccharide's influence on trpzip's gelation compared to other peptide hydrogels which can reversibly assemble and disassemble their crosslinked networks. Trpzip hydrogels show reversible shear recovery and self-healing behavior, so we next asked whether the addition of gellan gum might perturb this ability. Trpzip and trpzip-GG hydrogels were briefly exposed to 5% shear to break the network and then allowed to relax at 1% shear for 2 h. All hydrogel formulations showed reproducible recovery and returned to the starting modulus over at least three successive cycles.

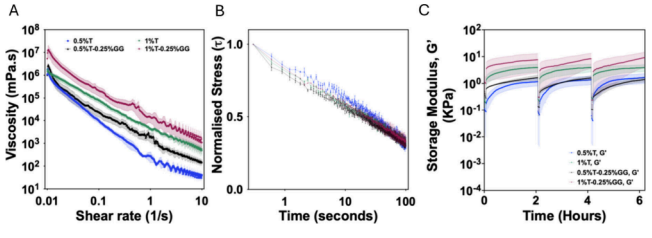

Figure 3. Viscoelasticity and self-healing of the hybrid hydrogels. A. Shear thinning behavior of trpzip-gellan gum (GG) hydrogels, $n = 3$. B. Normalized stress−relaxation for trpzip and hybrid trpzip-GG hydrogels, $n = 3$. C. Thixotropy assessment demonstrating shear recovery of the hydrogels involving exposure to 5% shear strain for 5 min, followed by reduction of shear strain to 1% for 2 h, repeated three times in succession, $n = 3$. Shaded areas indicate standard deviations between triplicate measurements.

To understand the morphology of these hybrid hydrogels, we performed cryogenic scanning electron microscopy (SEM) to visualize pore morphology. Both trpzip and trpzip−gellan gum hybrid materials show a network of irregular microscale pores, suggesting the addition of the polysaccharide does not disrupt the fractal-like ordering observed previously in pure trpzip materials[22] (Figure 4A). To confirm that this morphology is maintained through peptide-based secondary structures, we performed circular dichroism (CD) spectroscopy. Trpzip peptides' unique beta hairpin configuration resulted in a sharp peak occurring at 227 nm for both 0.5% and 1% (w/v) trpzip gels (Figure 4B). This primarily arose due to the indole rings found in tryptophan compactly packing into the folded zipper-like conformation. With the trpzip−gellan gum composite hydrogels, the peak has shown a shift from 227 to 220 and 223 nm (Figure 4C). Regardless of this change, the hybrid gels are still confirmed to be able to fold into beta sheets. A protein's secondary structure can be determined by the far-UV spectral signal, which appears in the wavelength range of 190−250 nm in CD spectroscopy,[32] and the composites peak wavelengths do fall into this range, thus supporting the assertion that beta sheet folding did occur. Within this range, peptide bonds act as a chromophore, causing signals to arise when in a folded environment.[33] The presence of β-sheet formation and other random coil structures gives rise to individual and characteristic magnitudes and shapes of CD spectra.

To support the formation of beta sheets in the trpzip gels and the hybrid gels, thioflavin-T (ThT) was used to tag the hydrogels prior to measuring the fluorescence intensity. Thioflavin-T is a fluorescence probe that is water soluble and is the conventional benzothiazole dye used for detecting amyloid fibrils (i.e., enhanced fluorescence is exhibited when it binds to amyloid fibrils).[34] Amyloid fibrils commonly form via soluble proteins which then assemble to form fibers that are insoluble and resistant to degradation. The most common use

https://doi.org/10.1021/acsmacrolett.5c00076
ACS Macro Lett. 2025, 14, 679−686

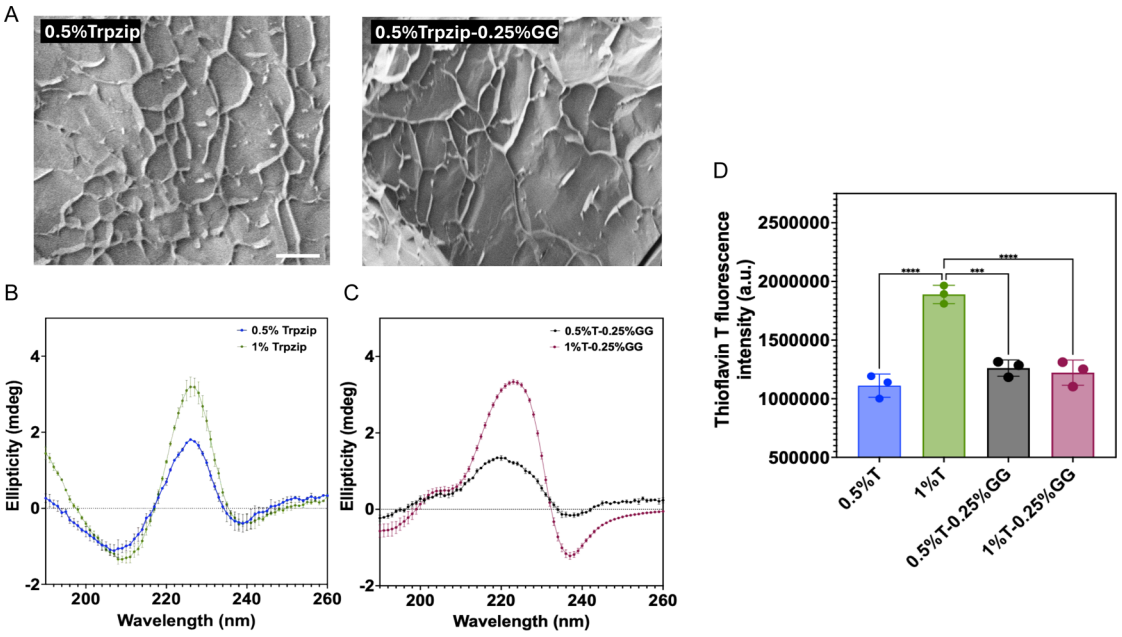

Figure 4. Physicochemical characterization of trpzip−gellan gum hydrogels. A. Cryogenic scanning electron micrographs demonstrating microporous nanofibrous matrices. Scale bar 40 μm. B. and C. Circular dichroism analysis of secondary structures in trpzip and trpzip−gellan gum gels, respectively, $n = 3$. D. Thioflavin T analysis to discern beta-sheet forming character of the trpzip and trpzip−gellan gum hybrid hydrogels, $n = 3$. *P*-values calculated using one-way ANOVA, $^{*}P < 0.05$, $^{**}P < 0.01$, $^{***}P < 0.001$, $^{****}P < 0.0001$, $n = 3$.

of ThT is for the diagnosis of amyloid fibrils in both in vitro and ex vivo assessments.[35] After tagging the gels with ThT and measuring their fluorescence intensities, we observe that as the concentration of trpzip increased there was a higher ThT signal corresponding to a higher qunatity of beta sheets (Figure 4D). However, as soon as gellan gum was introduced to the system, there was a decrease in the amount of beta sheet formation, presumably due to dilution as well as the gellan gum impeding formation of secondary structures.

To investigate the ability of the hydrogels to serve as effective tissue mimicking biomaterials, adipose derived stem cells (ADSCs) were encapsulated into the hydrogels, and their cytocompatibility as well as their morphometrics were analyzed. Cell studies were conducted with ADSCs encapsulated in both trpzip stand-alone gels at 0.5% (w/v) and trpzip−gellan gum gels at 0.5−0.25% GG (w/v). Bright-field imaging showed the effects on ADSCs after adding gellan gum to trpzip's hydrogel formation (Figure S1). We observe that the ADSCs prefer to remain as single cells in trpzip, and the addition of gellan gum promotes their migration and assembly/proliferation into aggregates. The ADSC aggregates displayed a more defined border, which indicates a preference for cell−cell interactions over cell−matrix interactions. This may be a useful property, for example, to coax cells so they assemble within the biomaterial during a process requiring the formation of aggregates, i.e., forming spheroids, cell condensation, chondrogenesis, etc. The tendency for the cells to prefer cell−cell interactions is unsurprising, considering the gellan gum is bioinert, thereby reducing the bioactive adhesive properties of the trpzip network. While these aspects may prove useful for the aforementioned applications, decorating the gellan gum with cell adhesion motifs is readily achievable using routine materials chemistry, which we would expect to lead to more spread morphologies such as the trpzip network alone.

To have a better understanding of the structure of ADSCs and to confirm their viability after two days of culture, they were released from the trpzip and trpzip composite matrices to perform live/dead imaging. As trpzip based hydrogels have low yield points, large cellular aggregates can be retrieved easily and can also be easily separated from the matrix with minimal damage to its mechanical integrity. This also circumvented the need for longer incubation times, or other chelation and enzyme mediated matrix dissolution methods, that is required when using materials such as Matrigel. Confocal microscopy was used for cell viability studies of the ADSCs encapsulated in the gels. The cells were fluorescently tagged, with the living cells appearing green and the dead cells appearing red. ADSCs encapsulated in the gels were confirmed to be highly viable (>90%) (Figure 5). Specifically, it was found that cell viability

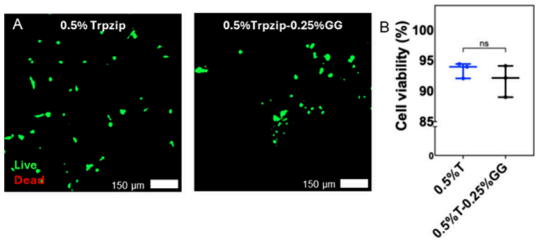

Figure 5. Adipose derived stem cell (ADSC) viability assessment. A. Live/dead imaging of ADSCs cultured in the trpzip and trpzip−gellan gum hydrogels after 2 days of culture. B. Quantification of cell viability assays, $n = 3$.

was higher for the trpzip standalone gel (~93%) compared to the trpzip−gellan gum gel (~91%). A possible reason for this is that gellan gum does not have any motifs for mammalian cells to adhere to while trpzip has a natural bioactivity. Nevertheless, viability >90% is indicative of good cytocompatibility

https://doi.org/10.1021/acsmacrolett.5c00076
ACS Macro Lett. 2025, 14, 679−686

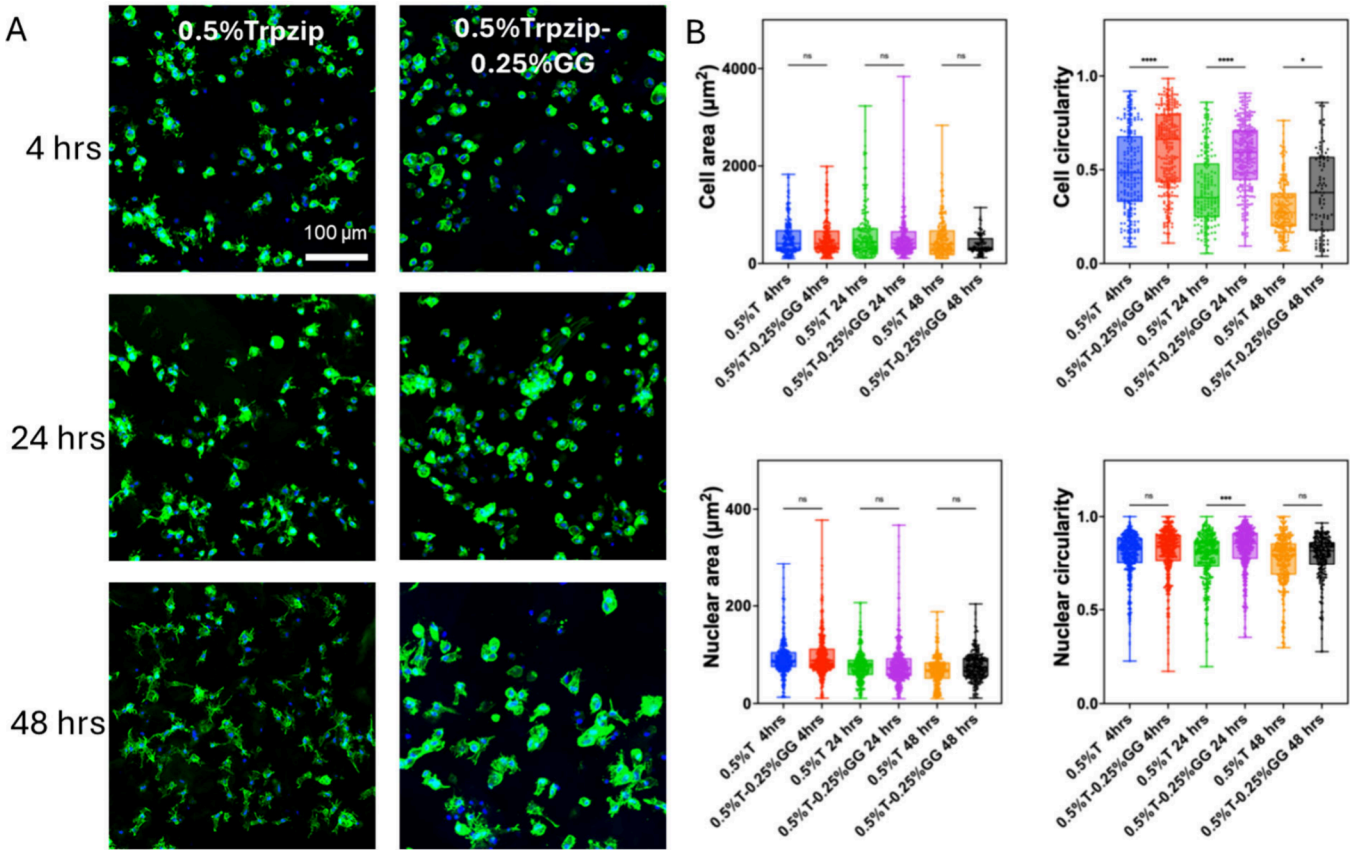

Figure 6. Morphometric analysis of adipose derived stem cells after culture in trpzip and trpzip−gellan gum hydrogels for 4, 24, and 48 h. A. Immunofluorescence microscopy images showing differences in cell morphology and adhesive characteristics, Scale bar = 100 μm. B. ADSC morphometric analysis: cell and nuclear area and circularity, n = 3 images. P-values calculated using one-way ANOVA, *P < 0.05, **P < 0.01, ***P < 0.001, ****P < 0.0001, n = 3.

supporting the use of trpzip−gellan gum hydrogels to support 3D cell culture.

The morphometrics of the encapsulated cells were also assessed through confocal microscopy. ADSCs were found uniformly dispersed within the trpzip and trpzip−gellan gum matrix at all timepoints, confirming there was no settling during the initial gelation period. Cells within the trpzip hydrogels elongate within the first 4 h demonstrating a spread morphology. In contrast, cells in the composite trpzip−gellan gum hydrogels were more circular. Overall, gellan gum appears to discourage cell elongation and spreading as determined by a decrease in area and aspect ratio, which is consistent with a low bioactivity of native gellan gum (Figures 6, S7, and S8). Concurrently, we see an increase in circularity, as expected. Nuclear morphology did not show any clear differences between the hydrogel conditions.

In this paper, we demonstrate a new class of hybrid natural and synthetic hydrogel based on a blend of trpzip nanofiber forming hydrogelators and gellan gum polysaccharides. The addition of gellan gum greatly enhances hydrogelation, leading to a more rigid hydrogel. The resultant materials maintain viscoelastic character and show good cytocompatibility, supporting cell viability and growth over time. The ability to rapidly form these hydrogels, while maintaining shear thinning and self-healing behavior, suggests that these formulations may be useful as biomaterials for cell encapsulation and extrusion for biofabrication and cell delivery.

MATERIALS AND METHODS

Materials. Synthetic peptide, trpzip (+), was purchased as the formate salt (purity >98%) from GenScript Biotech (Singapore) Pty Ltd. and used without further purification. Gellan gum (Gelzan CM, Cat: G1910) and DMEM (Cat: D5796) were purchased from Merck Pty. Ltd., Australia.

Hydrogel Preparation. Lyophilized trpzip peptides were dissolved in Milli-Q water at concentrations of 1% or 2% (w/v). To facilitate dissolution, magnetic stirring was performed on a hot plate set to 40 °C. Ion-mediated gelation was achieved by the addition of buffered cell culture media, resulting in a final concentration of 0.5% or 1%, respectively (w/v).

Trpzip−gellan gum hydrogels were prepared by dissolving 1% gellan gum in Milli-Q water with magnetic stirring at 60 °C. Gelation was triggered by mixing 1% gellan gum with cell culture media resulting in a final concentration of 0.5% GG. This solution was then combined with either 1% or 2% trpzip to a final concentration of 0.5% trpzip−0.25% GG or 1% trpzip−0.25% GG.

Trpzip and GG solutions were sterilized with UV light for 15 min prior to cell encapsulation.

Shear Rheology. Rheological measurements were performed on an Anton Paar MCR 302e Rheometer with parallel plate geometry (25 mm disc, 1 mm gap height, 560 μL of hydrogel). Oscillatory measurements were performed with 0.2% strain and a 1 Hz frequency at 37 °C unless specified otherwise. Viscosity flow curve tests were performed with a log ramp up rate from 0.01 to 10 shear rate (1 s^{-1}) over 10 min. Strain sweep tests were performed with a log ramp up rate from 0.02% shear strain up to 200% at a 1 Hz frequency over 10 min. Stress−relaxation tests were performed at 1% strain, after which the stress profile was normalized to the initial maximum stress. The decay half-time was calculated by determining the time at which stress

https://doi.org/10.1021/acsmacrolett.5c00076
ACS Macro Lett. 2025, 14, 679−686

was half of the initial normalized stress. Frequency sweeps were run with a log ramp up rate from 0.01 to 100 Hz with 0.2% strain. Thixotropy assessment was conducted by involving exposure to 5% shear strain for 5 min, followed by reduction of shear strain to 1% for 2 h, repeated three times in succession.

Cryogenic Scanning Electron Microscopy (Cryo-SEM). Trpzip and trpzip-GG hydrogels were applied to a cylindrical mold on a cryoSEM stub mounted on a cryoSEM holder. The holder was submerged in a liquid nitrogen bath at a slushy nitrogen freezing station (Quorum) for 10 min to ensure thorough vitrification of the sample. The frozen sample was then transferred under vacuum to a cryo-preparation chamber (Quorum PP3010T) precooled to −120 °C. Fracturing was performed within the chamber using a precooled scalpel to expose the internal structure of the hydrogel. The fractured sample was subsequently transferred to a Zeiss Crossbeam 550 Focus Ion Beam Scanning Electron Microscope. SEM imaging was performed at −120 °C using a 2 kV accelerating voltage with secondary electron detection.

Thioflavin T Fluorescence Assay. 100 μL of trpzip hydrogel samples in triplicates were aliquoted to a 96 well flat bottom plate and incubated overnight at 37 °C. A 100 μL portion of 200 μM Thioflavin-T dissolved in PBS was added to each well and incubated for 24 h. Further 1X PBS washes were done 3 times over 24 h. The gels were incubated in PBS, and fluorescence intensity was measured using a CLARIOSTAR multimode microplate reader (BMG Lab technologies, Melbourne, VIC, Australia) with 440/490 nm excitation/emission filters set. Thioflavin-T fluorescence data were normalized by subtracting Thioflavin-T only fluorescence intensity from hydrogel labelled thioflavin samples.

Circular Dichroism (CD) Spectroscopy. Hydrogel samples after overnight gelation were diluted in Milli-Q water at 0.5 mg/mL peptide concentrations. Far-UV CD spectra were recorded by using an Applied Photophysics Chirascan Plus CD spectrometer between 180 and 300 nm. CD spectra were recorded in 1 nm steps at 0.5 s per point. Samples were measured in a Starna Scientific 0.5 mm quartz cuvette. Final spectra were shown as the average of three scans with the subtraction of the baseline spectra.

Zeta Potential Measurements. The zeta potential of hydrogels was determined using the Zetasizer Ultra ZS instrument (Malvern, UK) by varying ionic concentrations. Hydrogel suspensions, trpzip, and GG solutions were added to DTS1070 cuvettes using 1 mL syringes, ensuring that no bubbles were formed. Hydrogel suspensions, trpzip, and GG solutions were equilibrated for 120 s at 37 °C before measurements in triplicates.

Trpzip and trpzip-GG hydrogels were formed using 1X DMEM for measurements involving ions, while trpzip solutions and trpzip-GG hydrogels formed with Milli-Q water were used for measurements devoid of ions.

Cell Culture and Seeding. hADSCs were cultured with high glucose Dulbecco's Modified Eagle Medium (DMEM) supplemented with 10% fetal bovine serum (FBS) and 1% penicillin/streptomycin. All cultures were maintained at 37 °C and 5% CO_2 and cells were used between passages 5 and 10. For 3D encapsulation of cells in trpzip and trpzip-GG hydrogel matrices, the cells were detached with 0.05% trypsin, counted, centrifuged down, and resuspended to 0.5 × 10^6 cells mL^{-1} of a hydrogel suspension. For all experiments, 100 μL of hydrogel−cell suspension was added to each well of a 96 well flat bottom plate and incubated for 1 h before adding 200 μL of expansion media to each well. Hydrogel samples were cultured with hADSCs in triplicates for 2 days and fixed with 4% PFA overnight.

Cell Viability Assay. hADSCs were detached from tissue culture flasks with 0.05% trypsin and seeded in hydrogels at a concentration of 0.5 × 10^6 cells/mL. The cell laden hydrogels were stiffened by incubation at 37 °C for 1 h before cell culture media was added. The viability was assessed using a Calcein-AM/Ethidium Homodimer-1 kit (ThermoFisher Scientific; cat #L3224) after two days of culture. For live/dead staining, Calcein-AM (0.5 μL/mL) and Ethidium-Homodimer-1 (2 μL/mL) were added to trpzip and trpzip-GG gels for 40 min before being washed three times with PBS prior to imaging.

Immunofluorescence Staining. Fixed 3D hydrogel cell samples were washed 3 times with 1X PBS at an interval of 4 h. Cells were permeabilized with 0.1% Triton X-100 overnight followed by blocking with 1% BSA and then washing 3 times with PBS at an interval of 4 h. Cells were stained for Phalloidin-488 (1:250 dilution) and DAPI (1:1000 dilution) for at least 24 h at room temperature. Finally, samples were washed with 1X PBS 3 times over 24 h and incubated in PBS at 4 °C until imaged. All confocal imaging was performed with a Zeiss LSM 800. A 10X objective with a 2.5 mm working distance was used to look deeper into the samples. Z-stack images of 50 slices of 2 μm intervals were taken at a resolution of 1024 × 1024. All the images were analysed using Fiji ImageJ software.

Statistical Analysis. GraphPad Prism (version 10.3.1) was used for the statistical analysis and plotting of all data. The sample size for all experiments was $n \geq 3$. Data are presented as mean ± standard deviation (SD). Student's *t*-test was used to analyze data between two groups. For comparing differences between multiple groups, one-way or two-way ANOVA with variance analysis was performed. Differences were determined to be statistically significant when $^{*}p < 0.05$, $^{**}p < 0.01$, and $^{***}p < 0.001$.

■ ASSOCIATED CONTENT

Supporting Information

The Supporting Information is available free of charge at https://pubs.acs.org/doi/10.1021/acsmacrolett.5c00076.

Bright-field images of cells, additional rheology data, and supporting immunofluorescence images with associated quantification of cell morphometrics (PDF)

■ AUTHOR INFORMATION

Corresponding Author

Kristopher A. Kilian − *School of Chemistry, Australian Centre for NanoMedicine, University of New South Wales (UNSW Sydney), Sydney, NSW 2052, Australia; School of Materials Science and Engineering, University of New South Wales (UNSW Sydney), Sydney, NSW 2052, Australia;* orcid.org/0000-0002-8963-9796; Email: k.kilian@unsw.edu.au

Authors

Riddhesh Doshi − *School of Chemistry, Australian Centre for NanoMedicine, University of New South Wales (UNSW Sydney), Sydney, NSW 2052, Australia*

Dhushanthan Mohanathas − *School of Chemistry, Australian Centre for NanoMedicine, University of New South Wales (UNSW Sydney), Sydney, NSW 2052, Australia*

Md. Shariful Islam − *School of Chemistry, Australian Centre for NanoMedicine, University of New South Wales (UNSW Sydney), Sydney, NSW 2052, Australia*

Juanfang Ruan − *Electron Microscopy Unit, Mark Wainwright Analytical Centre, University of New South Wales (UNSW Sydney), Sydney, NSW 2052, Australia*

Richard D. Tilley − *School of Chemistry, Australian Centre for NanoMedicine, University of New South Wales (UNSW Sydney), Sydney, NSW 2052, Australia; Electron Microscopy Unit, Mark Wainwright Analytical Centre, University of New South Wales (UNSW Sydney), Sydney, NSW 2052, Australia;* orcid.org/0000-0003-2097-063X

Complete contact information is available at: https://pubs.acs.org/10.1021/acsmacrolett.5c00076

Author Contributions

CRediT: **Riddhesh Doshi** data curation, formal analysis, investigation, methodology, visualization, writing - original

https://doi.org/10.1021/acsmacrolett.5c00076
ACS Macro Lett. 2025, 14, 679−686

draft; **Dhushanthan Mohanathas** data curation, formal analysis, investigation, writing - original draft.

Notes

The authors declare no competing financial interest.

■ ACKNOWLEDGMENTS

This work was supported through funding from the Australian Research Council Grant DP230101804 (K.A.K.) and the National Cancer Institute of the National Institutes of Health Grant R01CA251443 (K.A.K.). The authors gratefully acknowledge the support from Merck Life Science Pty. Ltd. in this work, through a generous scholarship for purchase of laboratory consumables in support of D.M. honours project in the School of Chemistry at UNSW Sydney. The authors acknowledge the help and support of staff at the Katharina Gaus Light Microscopy Facility (KGLMF), Structural Biological Facility (SBF), Electron Microscopy Unit (EMU), and Flow Cytometry Facility of the UNSW Mark Wainwright Analytical Centre.

■ REFERENCES

(1) Unal, A. Z.; West, J. L. Synthetic ECM: Bioactive Synthetic Hydrogels for 3D Tissue Engineering. *Bioconjug. Chem.* **2020**, *31* (10), 2253−2271.

(2) Singh, M. R.; Patel, S.; Singh, D. Natural Polymer-Based Hydrogels as Scaffolds for Tissue Engineering. In *Nanobiomaterials in Soft Tissue Engineering*; Elsevier, 2016; pp 231−260. DOI: 10.1016/B978-0-323-42865-1.00009-X.

(3) Mano, J. F.; Silva, G. A.; Azevedo, H. S.; Malafaya, P. B.; Sousa, R. A.; Silva, S. S.; Boesel, L. F.; Oliveira, J. M.; Santos, T. C.; Marques, A. P.; Neves, N. M.; Reis, R. L. Natural Origin Biodegradable Systems in Tissue Engineering and Regenerative Medicine: Present Status and Some Moving Trends. *J. R. Soc. Interface* **2007**, *4* (17), 999−1030.

(4) Catoira, M. C.; Fusaro, L.; Di Francesco, D.; Ramella, M.; Boccafoschi, F. Overview of natural hydrogels for regenerative medicine applications. *Journal of Materials Science: Materials in Medicine* **2019**, DOI: 10.1007/s10856-019-6318-7.

(5) Liu, Y.; Shariful Islam, M.; Bakker, A.; Li, Z.; Ajam, A. J.; Kruzic, J. A.; Kilian, K. Improving the Bioactivity and Mechanical Properties of Poly(Ethylene Glycol)-Based Hydrogels through a Supramolecular Support Network. *J. Mater. Chem. B* **2025**, *13*, 1286.

(6) Cai, M.-H.; Chen, X.-Y.; Fu, L.-Q.; Du, W.-L.; Yang, X.; Mou, X.-Z.; Hu, P.-Y. Design and Development of Hybrid Hydrogels for Biomedical Applications: Recent Trends in Anticancer Drug Delivery and Tissue Engineering. *Front. Bioeng. Biotechnol.* **2021**, DOI: 10.3389/fbioe.2021.630943.

(7) Choudhary, A.; Sharma, A.; Singh, A.; Han, S. S.; Sood, A. Strategy and Advancement in Hybrid Hydrogel and Their Applications: Recent Progress and Trends. *Adv. Eng. Mater.* **2024**, *26* (21), 2400944.

(8) Liu, S. Q.; Tian, Q.; Wang, L.; Hedrick, J. L.; Hui, J. H. P.; Yang, Y. Y.; Ee, P. L. R. Injectable Biodegradable Poly(Ethylene Glycol)/RGD Peptide Hybrid Hydrogels for in Vitro Chondrogenesis of Human Mesenchymal Stem Cells. *Macromol. Rapid Commun.* **2010**, *31* (13), 1148−1154.

(9) Mou, Z.-L.; Zhao, L.-J.; Zhang, Q.-A.; Zhang, J.; Zhang, Z.-Q. Preparation of Porous PLGA/HA/Collagen Scaffolds with Supercritical CO2 and Application in Osteoblast Cell Culture. *J. Supercrit. Fluids* **2011**, *58* (3), 398−406.

(10) Pillai, M. M.; Gopinathan, J.; Indumathi, B.; Manjoosha, Y. R.; Santosh Sahanand, K.; Dinakar Rai, B. K.; Selvakumar, R.; Bhattacharyya, A. Silk-PVA Hybrid Nanofibrous Scaffolds for Enhanced Primary Human Meniscal Cell Proliferation. *J. Membr. Biol.* **2016**, *249* (6), 813−822.

(11) Mohammed, A. A. Polyvinyl Alcohol Composite with Enhanced Mechanical and Biological Properties for Soft Tissue Application. *J. Biomim. Biomater. Biomed. Eng.* **2025**, *67*, 81−93.

(12) Milos, F.; del Campo, A. Polyacrylamide Hydrogels as Versatile Biomimetic Platforms to Study Cell-Materials Interactions. *Advanced Materials Interfaces* **2024**, DOI: 10.1002/admi.202400404.

(13) Mohanty, S.; Roy, S. Bioactive Hydrogels Inspired by Laminin: An Emerging Biomaterial for Tissue Engineering Applications. *Macromol. Biosci.* **2024**, *24* (11), 2400207.

(14) Tansik, G.; Stowers, R. Viscoelastic and Phototunable GelMA-Alginate Hydrogels for 3D Cell Culture. *MRS Adv.* **2024**, *9* (8), 505−511.

(15) Ajam, A.; Huang, Y.; Islam, M. S.; Kilian, K. A.; Kruzic, J. J. Mechanical and Biological Behavior of Double Network Hydrogels Reinforced with Alginate versus Gellan Gum. *J. Mech. Behav. Biomed. Mater.* **2024**, *157*, 106642.

(16) Bruggeman, K. F.; Rodriguez, A. L.; Parish, C. L.; Williams, R. J.; Nisbet, D. R. Temporally Controlled Release of Multiple Growth Factors from a Self-Assembling Peptide Hydrogel. *Nanotechnology* **2016**, *27* (38), 385102.

(17) Gelain, F.; Luo, Z.; Zhang, S. Self-Assembling Peptide EAK16 and RADA16 Nanofiber Scaffold Hydrogel. *Chemical Reviews* **2020**, *120*, 13434.

(18) Luo, R.; Wan, Y.; Liu, G.; Chen, J.; Luo, X.; Li, Z.; Su, D.; Lu, N.; Luo, Z. Engineering Self-Assembling Peptide Hydrogel to Enhance the Capacity of Dendritic Cells to Activate In Vivo T-Cell Immunity. *Biomacromolecules* **2024**, *25* (3), 1408−1428.

(19) Huang, W.; Dong, H.; Yan, Q.; Deng, T.; Li, X.; Zhao, Z.; Li, Z.; Wang, M.; Zhang, C.; Kong, B.; Shi, J.; Yuan, D. Disulfide-Rich Self-Assembling Peptides Based on Aromatic Amino Acid. *Small* **2025**, *21* (1), 2407464.

(20) Swain, J. W. R.; Yang, C. Y.; Hartgerink, J. D. Orthogonal Self-Assembly of Amphiphilic Peptide Hydrogels and Liposomes Results in Composite Materials with Tunable Release Profiles. *Biomacromolecules* **2023**, *24* (11), 5018−5026.

(21) Sawada, T.; Tsuchiya, M.; Takahashi, T.; Tsutsumi, H.; Mihara, H. Cell-Adhesive Hydrogels Composed of Peptide Nanofibers Responsive to Biological Ions. *Polym. J.* **2012**, *44* (6), 651−657.

(22) Nguyen, A. K.; Molley, T. G.; Kardia, E.; Ganda, S.; Chakraborty, S.; Wong, S. L.; Ruan, J.; Yee, B. E.; Mata, J.; Vijayan, A.; Kumar, N.; Tilley, R. D.; Waters, S. A.; Kilian, K. A. Hierarchical Assembly of Tryptophan Zipper Peptides into Stress-Relaxing Bioactive Hydrogels. *Nat. Commun.* **2023**, *14* (1), 6604.

(23) Kretsinger, J. K.; Haines, L. A.; Ozbas, B.; Pochan, D. J.; Schneider, J. P. Cytocompatibility of Self-Assembled β-Hairpin Peptide Hydrogel Surfaces. *Biomaterials* **2005**, *26* (25), 5177−5186.

(24) Jonker, A. M.; Löwik, D. W. P. M.; van Hest, J. C. M. Peptide- and Protein-Based Hydrogels. *Chem. Mater.* **2012**, *24* (5), 759−773.

(25) Liu, Y.; Gilchrist, A. E.; Heilshorn, S. C. Engineered Protein Hydrogels as Biomimetic Cellular Scaffolds. *Adv. Mater.* **2024**, *36* (45), 2407794.

(26) Chen, J.; Tao, N.; Fang, S.; Chen, Z.; Liang, L.; Sun, X.; Li, J.; Liu, Y.-N. Incorporation of Fmoc-Y Nanofibers into Ca-Alginate Hydrogels for Improving Their Mechanical Properties and the Controlled Release of Small Molecules. *New J. Chem.* **2018**, *42* (12), 9651−9657.

(27) Gong, X.; Branford-White, C.; Tao, L.; Li, S.; Quan, J.; Nie, H.; Zhu, L. Preparation and Characterization of a Novel Sodium Alginate Incorporated Self-Assembled Fmoc-FF Composite Hydrogel. *Mater. Sci. Eng. C* **2016**, *58*, 478−486.

(28) Cao, M.; Wang, Y.; Hu, X.; Gong, H.; Li, R.; Cox, H.; Zhang, J.; Waigh, T. A.; Xu, H.; Lu, J. R. Reversible Thermoresponsive Peptide-PNIPAM Hydrogels for Controlled Drug Delivery. *Biomacromolecules* **2019**, *20* (9), 3601−3610.

(29) Chaudhuri, O.; Gu, L.; Darnell, M.; Klumpers, D.; Bencherif, S. A.; Weaver, J. C.; Huebsch, N.; Mooney, D. J. Substrate Stress Relaxation Regulates Cell Spreading. *Nat. Commun.* **2015**, *6* (1), 6365.

(30) Nam, S.; Stowers, R.; Lou, J.; Xia, Y.; Chaudhuri, O. Varying PEG Density to Control Stress Relaxation in Alginate-PEG Hydrogels for 3D Cell Culture Studies. *Biomaterials* **2019**, *200*, 15−24.
(31) Farrell, K.; Joshi, J.; Kothapalli, C. R. Injectable Uncrosslinked Biomimetic Hydrogels as Candidate Scaffolds for Neural Stem Cell Delivery. *J. Biomed. Mater. Res. A* **2017**, *105* (3), 790−805.
(32) Greenfield, N. J. Using Circular Dichroism Spectra to Estimate Protein Secondary Structure. *Nat. Protoc.* **2006**, *1* (6), 2876−2890.
(33) Heinz, F.; Proksch, J.; Schmidt, R. F.; Gradzielski, M.; Koksch, B.; Keller, B. G. How Chromophore Labels Shape the Structure and Dynamics of a Peptide Hydrogel. *Biomacromolecules* **2024**, *25* (2), 1262−1273.
(34) Biancalana, M.; Koide, S. Molecular Mechanism of Thioflavin-T Binding to Amyloid Fibrils. *Biochim. Biophys. Acta* **2010**, *1804* (7), 1405−1412.
(35) Xue, C.; Lin, T. Y.; Chang, D.; Guo, Z. Thioflavin T as an amyloid dye: fibril quantification, optimal concentration and effect on aggregation. *Royal Society Open Science* **2017**, *4*, 160696.

https://doi.org/10.1021/acsmacrolett.5c00076
ACS Macro Lett. 2025, 14, 679−686